Bull Math Biol (2013) 75:2150–2166
DOI 10.1007/s11538-013-9885-7

Society for Mathematical Biology

ORIGINAL ARTICLE

Lattice-Free Models of Cell Invasion: Discrete Simulations and Travelling Waves

Michael J. Plank · Matthew J. Simpson

Received: 3 March 2013 / Accepted: 23 July 2013 / Published online: 17 August 2013

Abstract Invasion waves of cells play an important role in development, disease, and repair. Standard discrete models of such processes typically involve simulating cell motility, cell proliferation, and cell-to-cell crowding effects in a lattice-based framework. The continuum-limit description is often given by a reaction–diffusion equation that is related to the Fisher–Kolmogorov equation. One of the limitations of a standard lattice-based approach is that real cells move and proliferate in continuous space and are not restricted to a predefined lattice structure. We present a lattice-free model of cell motility and proliferation, with cell-to-cell crowding effects, and we use the model to replicate invasion wave-type behaviour. The continuum-limit description of the discrete model is a reaction–diffusion equation with a proliferation term that is different from lattice-based models. Comparing lattice-based and lattice-free simulations indicates that both models lead to invasion fronts that are similar at the leading edge, where the cell density is low. Conversely, the two models make different predictions in the high-density region of the domain, well behind the leading edge. We analyse the continuum-limit description of the lattice-based and lattice-free models to show that both give rise to invasion wave type solutions that move with the same speed but have very different shapes. We explore the significance of these differences by calibrating the parameters in the standard Fisher–Kolmogorov equation using data from the lattice-free model. We conclude that estimating parameters using this kind of standard procedure can produce misleading results.

Keywords Cell migration · Cell proliferation · Crowding effects · Travelling wave · Lattice-free

M.J. Plank (✉)
Department of Mathematics and Statistics, University of Canterbury, Christchurch, New Zealand
e-mail: michael.plank@canterbury.ac.nz

M.J. Simpson
Mathematical Sciences, Queensland University of Technology, Brisbane, Queensland, Australia
e-mail: matthew.simpson@qut.edu.au

1 Introduction

Invasion waves of cells are essential features of development (Druckenbrod and Epstein 2007; Nishiyama et al. 2012), repair (Maini et al. 2004a, 2004b) and disease (Sherratt 2000; Swanson et al. 2003). Such waves, or moving fronts of cells, can arise in systems that involve populations of cells that are motile and proliferate to a carrying capacity density. The combination of cell motility and carrying capacity-limited proliferation leads to invasion fronts that can move into vacant tissues leaving them uniformly occupied with cells behind the front. A typical image of an *in vitro* invasion front is shown in Fig. 1 where we see that the cell density is relatively low at the leading edge of the wave and relatively high well behind the leading edge.

The role of cell-to-cell crowding in invasion waves of cells has been demonstrated experimentally by labelling a few cells within the population and measuring properties of the trajectories of the labelled cells. Using this technique, Druckenbrod and Epstein (2007) showed that cells at the leading edge of an *in vivo* invasion wave were relatively motile, whereas cells located well behind the leading edge were relatively immotile. Similar results were observed by Cai et al. (2007) in an *in vitro* scratch assay using 3T3 Fibroblast cells. These observations highlight the importance of cell crowding and volume exclusion effects since isolated cells at the leading edge are free to move and proliferate, whereas crowded cells well behind the leading edge have less opportunity to move or proliferate.

Traditionally, experimental investigations describing invasion waves of cells have focused on measuring the speed of the advancing front (Maini et al. 2004a, 2004b). More recent advances in microscopy technologies, such as confocal microscopy, time-lapse imaging, and magnetic resonance imaging techniques, have allowed experimental investigations to report detailed measurements of individual cell behaviour within the bulk population. For example, Druckenbrod and Epstein (2007) measured the speed of the advancing front as well as recording the details of individual cell trajectories within the bulk population. Similarly, Young et al. (2004) measured the speed of an advancing wave front within an intact tissue culture system and sectioned the tissue so that they could study the movement of a few isolated cells within the bulk population. To keep pace with the changes in the way that experimental observations are reported, there has also been a change in the way

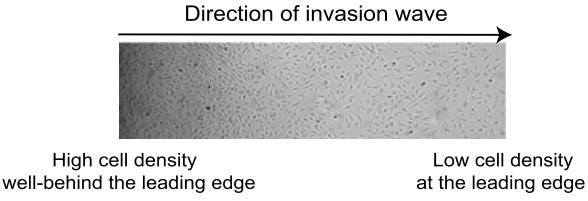

Fig. 1 Experimental image showing the spatial organisation of human umbilical vein endothelial cells in a typical scratch assay (Caruso et al. 2009). Reproduced with permission from PNAS. The image shows the distribution of cell density along an invasion wave of cells that is moving in the direction indicated. The cell density is low at the leading edge and individual cells are relatively unaffected by neighbouring cells whereas the cell density is high well behind the leading edge and individual cells are crowded by neighbouring cells

that mathematical models of invasion waves are designed and implemented to interpret such experimental observations. Traditionally, continuous partial differential equation (PDE) models related to the Fisher–Kolmogorov equation (Fisher 1937; Kolmogorov et al. 1937; Sherratt and Murray 1990; Sherratt 2000; Witelski 1994, 1995) were used to represent cell invasion since these models give rise to travelling wave solutions that are thought to represent invasion fronts (Maini et al. 2004a, 2004b). However, PDE-based models cannot provide any insight into the behaviour of individual cells within the invading population of cells. To overcome this limitation, individual-based, random walk models of cell motility and cell proliferation have become increasingly popular (Anderson and Chaplain 1998; Codling et al. 2008; Othmer et al. 1988).

One approach to modelling cell invasion in a discrete random walk framework is to use a lattice-based approach where individual agents (cells) on a lattice undergo motility and proliferation events. Crowding effects can be incorporated by ensuring that each lattice site can be occupied by, at most, one cell. Such a model, on a one-dimensional lattice, was considered by Callaghan et al. (2006) who showed that discrete simulations appeared to mimic invasion wave like behaviour. A similar model, on a two-dimensional square lattice, was studied by Simpson et al. (2010) who derived an approximate conservation statement and showed that the continuum limit of the model is a generalisation of the Fisher–Kolmogorov equation. All lattice-based models of collective cell behaviour make a major simplifying assumption that the movement and proliferation of individual cells is restricted to an artificial, predefined lattice. This limitation was recently highlighted by Plank and Simpson (2012) who considered a two-dimensional discrete model of a tissue growth experiment. Their results revealed some of the artificial features of lattice-based models, which always predict that the population of cells will grow to confluence by aligning along the underlying lattice structure. In contrast, real images of the same kinds of experiment (e.g. Tremel et al. 2009) show that cells are arranged less regularly as they grow to confluence.

In this work, we build on recent advances by simulating and analyzing a lattice-free random walk model with crowding effects that is motivated by observations in cell biology (Plank and Simpson 2012). Unlike some recent lattice-free models that neglect proliferation (e.g. Dyson et al. 2012; Bruna and Chapman 2012a, 2012b), we consider a lattice-free model incorporating cell motility, cell proliferation and realistic crowding effects. Discrete simulations illustrate the potential for the model to replicate moving fronts that are similar to invasion waves of cells. We present a corresponding PDE-based model that describes the average behaviour of lattice-free simulations, and we show that the PDE model gives rise to solutions that mimic the essential features of an invasion wave of cells. Using a combination of numerical simulation and analysis, we show that the invasion fronts associated with the lattice-free PDE description have the same invasion speed properties as the Fisher–Kolmogorov equation, but that the shape of the invasion front is very different. We highlight the importance of these differences by mimicking a standard procedure to calibrate the parameters in the Fisher–Kolmogorov equation using our more realistic lattice-free data. This exercise shows that a standard calibration procedure can produce misleading results.

2 Discrete Models

2.1 Lattice-Based Model

We consider a lattice-based model of cell motility and proliferation that has been described previously (Plank and Simpson 2012). Briefly, we consider a two-dimensional square lattice with lattice spacing Δ, which is assumed to correspond to the cell diameter (Simpson et al. 2013a, 2013b). In any one realisation, the occupancy of site (i, j) is $\bar{C}_{i,j}$, with $\bar{C}_{i,j} = 1$ for an occupied site, and $\bar{C}_{i,j} = 0$ for a vacant site. Simulations are performed using discrete time steps of duration τ and a random sequential update method is used to implement an unbiased motility mechanism so that each cell is given, on average, an opportunity to undergo a motility event with probability $P_m \in [0, 1]$ per time step (Chowdhury et al. 2005). Similarly, each cell is given, on average, an opportunity to undergo a proliferation event with probability $P_p \in [0, 1]$ per time step. A proliferative cell at site (i, j) attempts to place a daughter cell at site $(i \pm 1, j)$ or $(i, j \pm 1)$, each with equal probability $1/4$. Crowding effects are incorporated into the model by ensuring that potential motility and proliferation event that would place a cell on an occupied site are aborted.

2.2 Lattice-Free Model

We consider a new lattice-free model of cell motility and proliferation that was introduced recently by Plank and Simpson (2012). In this model, a cell can occupy any location in continuous two-dimensional space provided there is sufficient space available to accommodate it. The position of the centre of the ith cell is (x_i, y_i) for $i = 1, \ldots, N$. A random sequential update method is used to implement unbiased motility and proliferation mechanisms so that during any time step, of duration τ, each cell is, on average, given the opportunity to move with probability $P_m \in [0, 1]$ (Chowdhury et al. 2005). Each cell attempts to move a distance Δ in a random direction $\theta \in [0, 2\pi)$ and we assume that each cell is a circle of diameter Δ. To enforce crowding effects, any motility event where the cell's attempted path

$$(x_i, y_i) + s\Delta(\cos\theta, \sin\theta), \quad \text{where } s \in [0, 1],$$

comes within a distance Δ of any other cell's centre is aborted. Each cell is also given the opportunity to proliferate with probability $P_p \in [0, 1]$ during each time step. A proliferative cell will attempt to divide into two daughter cells that are separated by distance Δ along an axis of randomly chosen direction $\theta \in [0, \pi]$. Attempted proliferation events are aborted if the path connecting the daughter cells' target positions,

$$(x_i, y_i) + s(\Delta/2)(\cos\theta, \sin\theta), \quad \text{where } s \in [-1, 1],$$

comes within a distance Δ of any other cell's centre (Plank and Simpson 2012).

This lattice-free model is based on relatively simple mechanisms for cell motility, cell proliferation, and cell-to-cell crowding. It would be possible to extend this discrete model in various ways. For example, here we investigate the simplest possible mechanism where the direction of each potential motility and proliferation event is

chosen uniformly at random in $[0, 2\pi)$. This is analogous to a lattice-based blind random walk (Landman and Fernando 2011). One alternative model would be to assess the relative positions of neighbouring cells and to choose the direction of motility or proliferation events at random from the available directions. This would be analogous to a lattice-based myopic random walk (Landman and Fernando 2011). We anticipate that altering these mechanisms in the discrete model would lead to a different continuum-limit description (Landman and Fernando 2011) and we leave this extension for future work.

3 Continuum Models

The continuum descriptions of the lattice-based and lattice-free models have been derived previously (Simpson et al. 2010; Plank and Simpson 2012). The continuum description of the average cell density, $C(x, y, t)$, is given by a reaction–diffusion PDE of the form

$$\frac{\partial C}{\partial t} = D\nabla^2 C + f(C), \tag{1}$$

where D is the diffusivity and $f(C)$ is the local proliferation rate at density C. The diffusivity is related to the probability of movement P_m in the individual-based model via $D = P_m\Delta^2/(4\tau)$ (Plank and Simpson 2012). If the initial condition, $C(x, y, 0)$, is independent of the vertical coordinate y, and either periodic or reflecting boundary conditions are applied on both boundaries parallel to the x coordinate, the solution of Eq. (1) is independent of y for all $t > 0$ and we have $C(x, y, t) = C(x, t)$ (Simpson et al. 2010). These kinds of initial conditions and boundary conditions are relevant when considering cell invasion along a narrow channel, such as the experimental image in Fig. 1 and many other experimental investigations (e.g. Khain et al. 2011; Maini et al. 2004a, 2004b). In these cases, Eq. (1) can be applied in a one-dimensional Cartesian geometry where we have $\nabla^2 C = \partial^2 C/\partial x^2$.

The PDE description of the lattice-based and lattice-free models effectively makes a standard mean-field assumption that there are no short-range correlations in the locations of cells (Baker and Simpson 2010; Bolker and Pacala 1997; Law and Dieckmann 2000). This assumption is reasonable provided that proliferation events are relatively rare, i.e. $P_p/P_m \ll 1$ (Simpson et al. 2010; Plank and Simpson 2012). When this restriction is violated, spatial clustering of cells can occur, and short-range correlations cannot be neglected (Baker and Simpson 2010). For many applications in cell biology, the timescale of proliferation is much greater than the timescale of motility, so we have $P_p/P_m \ll 1$ (Simpson et al. 2010) and we can reasonably neglect the influence of short-range correlations (Deroulers et al. 2009).

The continuum limit of the lattice-based model, described in Sect. 2.1, is given by Eq. (1) with a logistic growth term (Simpson et al. 2010),

$$f(C) = \lambda C\left(1 - \frac{C}{K}\right), \tag{2}$$

where λ is per capita proliferation rate at low density ($C \to 0^+$) and $K = 1/\Delta^2$ is the density of a fully occupied square lattice. The proliferation parameter λ is related

to the probability of proliferation P_p in the individual-based model via $\lambda = P_p/\tau$. In one dimension, the continuum limit of the lattice-based model is, therefore, the standard Fisher–Kolmogorov equation (Fisher 1937; Kolmogorov et al. 1937) and previous research has shown that averaged simulation data from this discrete model corresponds with the solution of Eq. (1) with a logistic source term (Simpson et al. 2010).

If, instead of being restricted to a lattice, the cells in the discrete model move in continuous space, but are still subject to the crowding mechanism described in Sect. 2.2, the proliferation rate is well approximated by Plank and Simpson (2012)

$$f(C) = \lambda C \prod_{i=1}^{\frac{C}{Kd^2}-1} \left(1 - \frac{2d^2}{(1-\pi d^2)^i}\right), \tag{3}$$

where d is the ratio of the cell diameter to the length of the domain. Equation (3) was derived in our previous work, which was restricted to a uniformly populated domain without the development of spatially variable proliferative fronts of cells (Plank and Simpson 2012). In brief, the derivation of Eq. (3) involves considering how a series of proliferation events leads to a reduction in the amount of available space. This reduction in available space depends on the cell diameter Δ relative to the size of the domain. In a typical experimental scenario, the domain is large relative to the cell diameter and, therefore, $d \ll 1$. For a typical cell diameter of $\Delta = 25$ μm and domain length $L = 15$ mm (Simpson et al. 2013a, 2013b), we have $d = 0.002$. For such small values of d, the proliferation rate $f(C)$ in Eq. (3) is insensitive to d and $f(C)$ converges as $d \to 0$.

To evaluate the product in Eq. (3) the upper limit, $C/(Kd^2) - 1$, of the index must be approximated as an integer. Because d is small, $C/(Kd^2) - 1$ is typically large and it makes a negligible difference whether it is approximated as the nearest integer, the floor (nearest smaller integer) or the ceiling (nearest larger integer). We checked that all results presented here were insensitive to this choice.

All PDE results presented here use a fixed value of $d = 0.005$; we have checked that reducing the value of d does not affect the results. Figure 2 shows the two proliferation functions given in Eqs. (2) and (3). Note that the low-density per capita proliferation rate ($f'(0)$ in Fig. 2(a) or equivalently $\lim_{C\to 0^+} f(C)/C$ in Fig. 2(b)) is the same in both models.

In both the lattice-based and lattice-free models, the parameter K is a reference density and is related to the cell diameter Δ since $K = 1/\Delta^2$. In the lattice-based framework, K has a well-defined physical interpretation: in the discrete model, this density corresponds to a fully occupied lattice, which means that no further proliferation events are permitted (Plank and Simpson 2012); in the continuous description we have $f(K) = 0$, which means that K is the maximum density or carrying capacity density. In contrast, the lattice-free proliferation model does not have a well-defined carrying capacity density as $f(C) > 0$ for all C, so the density can, in principle, continue to grow without bound (Plank and Simpson 2012). In practice, however, $f(C)$ becomes extremely small as C increases, so the density C does not reach K on biologically relevant timescales (Plank and Simpson 2012). The choice of reference density is arbitrary. For example, we could have chosen the reference density

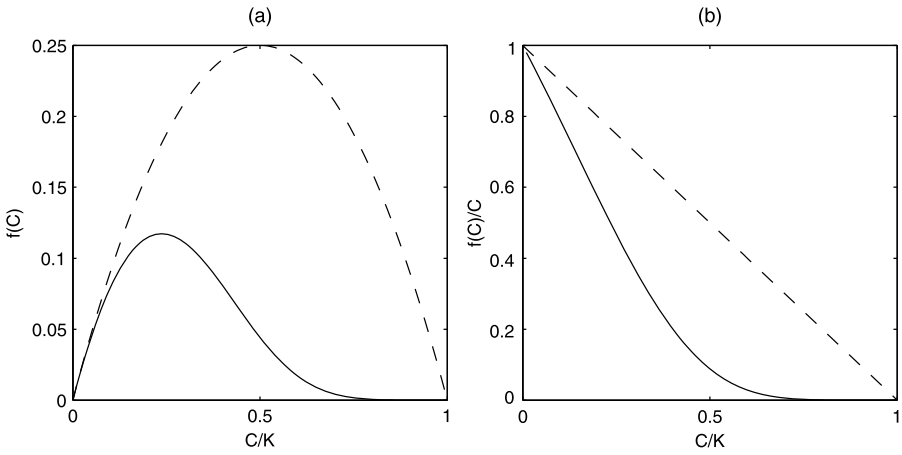

Fig. 2 Proliferation rates for the logistic growth model (Eq. (2), *dashed*) and the lattice-free model (Eq. (3), *solid*) as a function of C/K: (**a**) total proliferation rate $f(C)$; (**b**) per capita proliferation rate $f(C)/C$. Parameter values: $\lambda = 1$, $d = 0.005$. Changing λ simply scales $f(C)$ linearly; reducing d has a negligible effect on $f(C)$

to correspond to the carrying capacity density for a hexagonal arrangement of cells, which is the theoretical upper bound for the density in the discrete lattice-free model. Instead, we chose the reference density to correspond to the carrying capacity density for a square packing arrangement since this made it very easy to compare the lattice-based and lattice-free models.

Equation (3) provides an accurate prediction of the average increase in cell density for a spatially uniform initial condition (Plank and Simpson 2012). However, it remains to be examined whether the PDE description of the lattice-free model, Eq. (1) with (3), accurately predicts the averaged behaviour of the lattice-free model for problems with spatially varying cell density profiles, such as moving invasion fronts. We will examine this question, in detail, in Sect. 4. One of the advantages of working with the continuum limit description of the discrete model is that Eq. (1) can be non-dimensionalised so that the solutions are, in effect, independent of the parameter values λ, D and K. In the following analysis, we will always present solutions with $\lambda = D = K = 1$, but we note that all our results can be used to represent any other parameter values by an appropriate rescaling of x, t and C (Canosa 1973; Murray 2002).

4 Results

4.1 Comparing Lattice-Based and Lattice-Free Models: Short-Term Behaviour

We begin demonstrating qualitative differences between the lattice-based and lattice-free models by inspecting snapshots of discrete simulations (Fig. 3). Results in Fig. 3(a)–(c) show snapshots of a lattice-based simulation where the region $x \leq x_0$ is initially uniformly occupied at a relatively low density, and the remainder of the

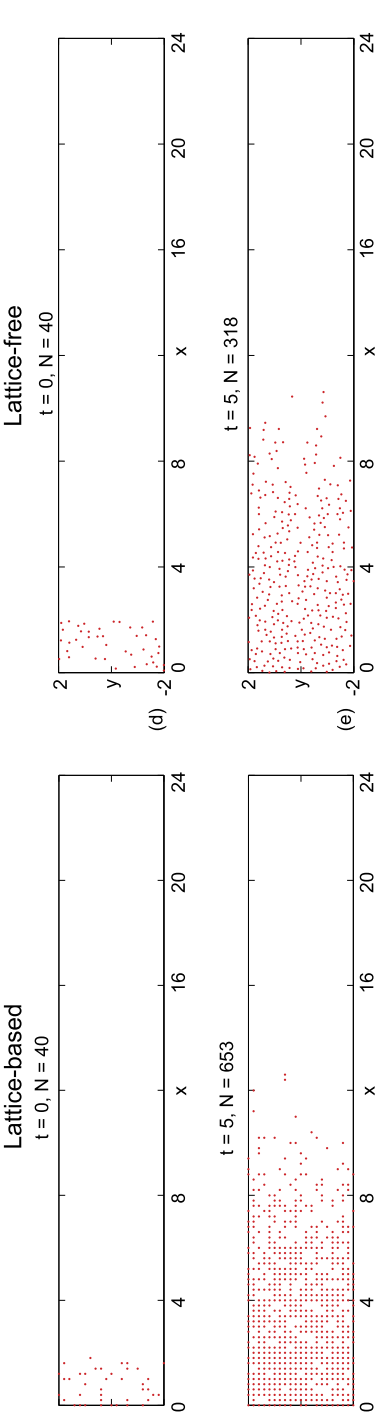

Fig. 3 Individual-based simulations of: (**a**)–(**c**) the lattice-based model; (**d**)–(**f**) the lattice-free model (Plank and Simpson 2012). Cell motility and proliferation events are aborted whenever there is insufficient space available. Initial condition: N_0 cells are placed at random in the region $0 \leq x \leq x_0$ such that the distance between any pair of cells is never less than one cell diameter Δ. Parameter values: probability of movement $P_m = 1$; probability of proliferation $P_p = 0.01$; $x_0 = 2$; $N_0 = 40$; $\Delta = 0.2$; $\tau = 0.01$ (the values of Δ and τ are dimensionless values chosen such that $\lambda = D = 1$ in the continuum limit)

domain, $x > x_0$, is initially vacant. The simulations show the influence of cell motility and proliferation events as individual cells move along the domain and proliferate so that the total number of cells in the system increases with time. The net result of the combination of motility and proliferation events is the formation of a front that moves in the positive x direction. As time increases, the density increases quickly behind the front so that almost all lattice sites are occupied. The alignment of cells along the lattice is clearly visible in Fig. 3(c), whereas the experimental image in Fig. 1 shows that cells behind the front less regularly distributed.

Results in Fig. 3(d)–(f) show an equivalent set of lattice-free simulations, using the same initial conditions and parameters as in the lattice-based simulations. The lattice-free simulations also indicate the development of an invasion front that moves in the positive x direction. The density of cells behind the front increases with time; however, the total population growth is much slower than in the corresponding lattice-based simulations. For example, at $t = 1000$, the lattice-based population has grown to almost double the size of the lattice-free population. Importantly, the cells behind the front in the lattice-free simulations are not regularly aligned, and instead are arranged in an irregular pattern. This is consistent with the experimental image in Fig. 1. Despite these differences between the lattice-based and lattice-free simulations in Fig. 3, the location of the leading edge of the front appears to be similar in both models. We will now investigate these observations by comparing simulation data to the solutions of the continuum-limit descriptions.

To obtain average cell density profiles, we perform M identically prepared realizations of the simulations shown in Fig. 3. In the mth realisation, we count the number of cells $N_m(x,t)$ whose horizontal coordinate lies within the interval $[x, x+\delta x)$ at time t. The average cell density $\langle C(x,t)\rangle$ is calculated by averaging over the M realizations to give

$$\big\langle C(x,t)\big\rangle = \frac{1}{M y_{\max}\delta x}\sum_{m=1}^{M} N_m(x,t),$$

where $y_{\max}$ is the height of the domain (so that $y_{\max}\delta x$ is the area of the thin strip $[x, x+\delta x)$). This is effectively a double average over the vertical coordinate y and over the M realizations. Increasing either M or $y_{\max}$ increases the number of cells used to estimate $\langle C(x,t)\rangle$. Previous work has explicitly investigated how the fluctuations in the $\langle C(x,t)\rangle$ density profile decrease as either M or $y_{\max}$ are increased (Simpson et al. 2011).

Previous investigations have confirmed that averaged density data from the lattice-based model match the solution of Eq. (1) with the traditional logistic growth term (Simpson et al. 2010) and we do not repeat this comparison here. Instead, we focus on comparing averaged cell density data from the lattice-free model with numerical solutions of Eq. (1) with the lattice-free source term, Eq. (3). To match the individual-based simulation data, we specify the initial condition for Eq. (1) to be a constant density for $0 < x \le x_0$ and zero density for $x_0 < x \le L$:

$$C(x,0) = \begin{cases} C_0, & x \le x_0, \\ 0, & x > x_0, \end{cases} \tag{4}$$

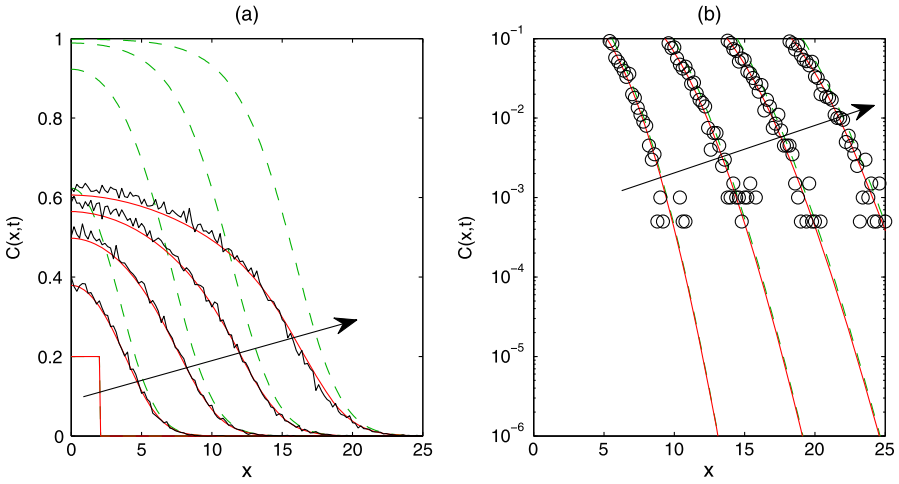

Fig. 4 Averaged cell density profiles from simulations of the individual-based lattice-free model (*black curves/circles*) superimposed on the solution of Eq. (1) with the lattice-based logistic growth term (*dashed green*) and the lattice-free growth term (*solid red*): (**a**) on a linear density axis; (**b**) on a logarithmic density axis showing the leading edge ($C(x,t) < 0.1$) of the invasion front (simulation data are plotted as disconnected points because points for which $C(x,t) = 0$ cannot be plotted on the logarithmic axis). Density profiles $C(x,t)$ are shown at $t = 0.0, 2.5, 5.0, 7.5, 10.0$ with *the arrow* showing the direction of increasing t. The individual-based simulations are the same as shown in Fig. 3(d)–(f); $C(x,t)$ is the density at horizontal position x and time t, averaged vertically and over $M = 100$ identically prepared simulations. Parameter values: $\lambda = D = K = 1$. The initial condition is given by Eq. (4) with $C_0 = 0.2$, $x_0 = 2$. PDEs were solved on a domain of length $L = 50$ with mesh spacing $\delta x = 0.1$ (Color figure online)

We impose zero-flux boundary conditions on $x = 0$ and $x = L$ and take the domain length L to be sufficiently large that the density at $x = L$, $C(L,t)$, remains negligibly small over the timescale investigated. Numerical solutions of Eq. (1) were obtained using the MATLAB® *pdepe* routine, which uses the method of lines (Chapra and Canale 1998) and the *ode15s* ODE solver (Shampine and Reichelt 1997), on a mesh with spacing δx.

The averaged density data for the lattice-free simulations are shown in Fig. 4. This confirms that the average density profile from the individual-based lattice-free model grows and spreads along the domain to form a front that moves in the positive x direction. Superimposed on the simulation data are two solutions of Eq. (1): one solution corresponds to the lattice-based logistic growth term, given by Eq. (2), and the other solution corresponds to the lattice-free growth term, given by Eq. (3). The solution of the PDE with the lattice-free growth term provides an excellent match to the averaged lattice-free simulation data, whereas the solution of the PDE with the traditional logistic growth term does not.

Although the solution of Eq. (1) with the lattice-free growth term is very different to the equivalent solution of with the lattice-based logistic growth term in the high-density region of the domain, the two solutions match very closely at the invading front, where the density is low (see Fig. 4(b), which shows the leading-edge part of the solution on a logarithmic axis). This is consistent with the discrete snapshots in Fig. 3, which show that the lattice-based and lattice-free simulations behave

differently well behind the invasion front, but behave similarly at the leading edge. These similarities and differences can be explained by considering the per capita proliferation rate, $f(C)/C$, for the two different proliferation models (Fig. 2(b)). In the individual-based models, $f(C)/(\lambda C)$ is equivalent to the proportion of attempted proliferation events that are successful at density C. As shown in Fig. 2(b), this proportion decreases from 1 in the low-density limit ($C \to 0^+$) toward 0 as the population density increases. Comparing the two curves confirms that crowding effects are stricter in the lattice-free model than in the lattice-based model, as the per capita proliferation rate decreases more rapidly with C.

4.2 Comparing Lattice-Based and Lattice-Free Models: Long-Term Behaviour

In Sect. 4.1, we established that solutions of Eq. (1) with the lattice-free source term, given by Eq. (3), provide an excellent match to averaged density data obtained from the lattice-free simulations over a relatively short timescale. Simulating the individual-based lattice-free model for longer time periods becomes very computationally expensive as the population grows (Plank and Simpson 2012). For example, the lattice-free simulation results in Fig. 3 required approximately 100 times the computational time of the equivalent lattice-based simulations; this cost increases rapidly for longer time periods due to the growing population size. We therefore restrict our investigation of long-term behaviour to the continuum-limit model given by Eq. (1) without performing long-term lattice-free discrete simulations.

It is well known that PDEs of the form of Eq. (1) on an infinite domain, $-\infty < x < \infty$ can give rise to travelling-wave solutions for a range of $f(C)$ (Murray 2002; Canosa 1973). For our initial conditions and source terms, we expect travelling-wave solutions moving at the minimum wave speed $c_{\min} = 2\sqrt{f'(0)D}$ (Murray 2002), which is an increasing function of the diffusivity, D, and the low-density per capita proliferation rate, $f'(0) = \lambda$.

The continuum-limit descriptions of both the lattice-based and the lattice-free model have the same low-density per capita proliferation rate, $f'(0) = \lambda$. Physically, the reason that the two models share the same $f'(0)$ is that crowding effects, which are handled differently by the two models, are unimportant at low cell density (Plank and Simpson 2012). Therefore, the behaviour of the continuum-limit description at low density, for example at the leading edge of an invasion wave, is the same for both models. This idea is supported by the short-term discrete and continuum results presented in Figs. 3 and 4, which show that the low-density leading edges of the solutions of the two models are almost indistinguishable. However, the behaviour at high density, for example well behind the leading edge of a invasion wave, is different since the two models handle crowding effects differently. These differences are reflected in the source terms $f(C)$, given by Eqs. (2) and (3). In summary, we expect that the long-term speed of the invasion front will be the same for the lattice-based and lattice-free models, but the shape of the invasion front and the long-term dynamics in the high-density region of the domain will be quite different.

Figure 5 shows numerical solutions of Eq. (1) with the lattice-based logistic proliferation source term, given by Eq. (2), and the lattice-free proliferation source term, given by Eq. (3). Both solutions appear to develop an invasion front moving with

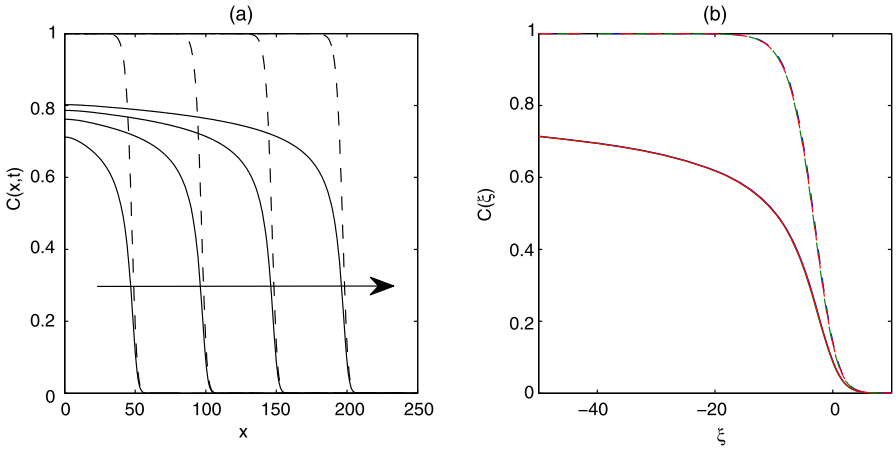

Fig. 5 Long-term solutions of Eq. (1) with the lattice-based logistic growth term (Eq. (2), *dashed*) and the lattice-free growth term (Eq. (3), *solid*): (**a**) density profiles at $t = 25, 50, 75, 100$ (*the arrow* shows the direction of increasing t); (**b**) density profiles at $t = 50$ (*blue*), $t = 75$ (*green*) and $t = 100$ (*red*) plotted against the travelling coordinate $\xi = x - ct$ with $c = 2\sqrt{\lambda D}$; the three curves lie on top of one another and are indistinguishable. Parameter values: $\lambda = D = K = 1$. The initial condition is given by Eq. (4) with $C_0 = 0.2$, $x_0 = 5$. PDEs were solved on a domain of length $L = 300$ with mesh spacing $\delta x = 0.2$ (Color figure online)

constant speed. This can be seen in Fig. 5(b), in which the solutions are plotted as a function of the travelling coordinate $\xi = x - ct$, with $c = 2\sqrt{\lambda D}$. The solutions almost collapse onto a single curve, indicating that a constant speed, constant shape invasion front profile has formed, and the speed of the moving fronts is very close to the theoretically expected value of $c = 2\sqrt{\lambda D}$. Solutions for even larger values of t are not shown, but these also collapse onto the same curves shown in Fig. 5(b). Although the speeds of the moving invasion fronts are the same, their shapes are very different for the two models. The lattice-free solution develops a much longer tail behind the leading edge of the wave. In this region, proliferation in the lattice-free model becomes extremely slow, but remains non-zero.

4.3 Comparing Lattice-Based and Lattice-Free Models: Estimating Parameter Values from Experimental Data

Parameters such as the diffusivity D, the low-density proliferation rate λ and the carrying capacity density K are difficult to measure directly and can vary considerably between cell types and different extracellular environments (Swanson et al. 2008). Estimates for these parameters are often estimated using data from cell biology experiments, such as scratch assays and barrier assays (Caruso et al. 2009; Simpson et al. 2013a, 2013b). A standard approach is to estimate these parameters is to use a least-squares approach to fit the solution of the Fisher–Kolmogorov equation to experimental cell density data (Sengers et al. 2007, 2009). Alternatively, the same least-squares procedure could be used to fit the lattice-free PDE model described here. In this section, we compare the results using both the lattice-based and lattice-free PDE models to estimate parameters from lattice-free simulation data. Our goal

is to investigate the accuracy of parameter estimates from both models when applied to noisy density profiles, such as the density profiles produced by our discrete lattice-free simulations. Typically, cell biology experiments can only be run over relatively short time scales that may not be sufficiently long to see the formation of constant speed, constant shape travelling fronts (Sengers et al. 2007, 2009). Therefore, we restrict our attention here to experimentally relevant time scales which may not be long enough to observe such fronts.

We used the averaged cell density data $\langle C(x,t)\rangle = C_{\text{sim}}(x,t)$ from the discrete lattice-free model, shown previously in Fig. 4, to estimate the parameters in the lattice-based PDE and the lattice-free PDE. The true parameter values in the simulation are $\lambda = D = K = 1$. For each PDE model, and for a given experimental time point T, we found the values of λ, D, and K that minimised the sum of squared differences R between the numerical solution of the PDE ($C_{\text{PDE}}(x, T; \lambda, D, K)$) and the simulation data ($C_{\text{sim}}(x, T; 1, 1, 1)$):

$$R(\lambda, D, K) = \sum_{i=1}^{n} \big(C_{\text{PDE}}(x_i, T; \lambda, D, K) - C_{\text{sim}}(x_i, T; 1, 1, 1)\big)^2. \tag{5}$$

The function R was minimised over λ, D, and K using the MATLAB® *fminsearch* routine, which uses the simplex search method (Lagarias et al. 1998). Initial estimates for the parameters for *fminsearch* were set as $\lambda = D = K = 1$, but the results are robust to different initial estimates. Recall that any solution of Eq. (1) can be rescaled to match any combination of parameters, λ, D and K. However, such a rescaling affects the timescale of the model. Using experimental data from 3T3 fibroblast cells, Simpson et al. (2013a, 2013b) estimated $\lambda = 0.05$ hr^{-1}, which means that 1 unit of dimensionless time t corresponds to $1/\lambda = 20$ hr. This gives an approximate scaling for t and allows us to restrict attention to experimentally relevant timescales. We consider time points T up to $T = 10$, which corresponds to approximately 200 hr, which is at the upper end of achievable *in vitro* experiments (Sengers et al. 2007, 2009; Simpson et al. 2013a, 2013b).

Figure 6 shows the least-squares solutions of the two PDE models superimposed on the simulation data at time $T = 5$. Both PDE models provide a good fit to the simulation data suggesting that it would not be possible to distinguish which is the correct model using noisy density data. Table 1 shows the estimated parameter values for the two models, for four different experimental durations. Parameter estimates for the lattice-free PDE are reasonably accurate, within approximately 5 % of the true values. In contrast, parameter estimates for the lattice-based PDE are far less accurate and consistently underestimate λ and K, while overestimating D. Furthermore, the lattice-based parameter estimates vary considerably depending on the duration of the experiment. This indicates that there is no unique combination of parameters in the lattice-based PDE that matches the data over the entire time period.

Although it is not surprising that the lattice-free PDE provides more accurate parameter estimates for discrete data obtained from a lattice-free simulation, these results illustrate that caution should be exercised when following the standard approach of estimating population-level PDE parameters by fitting PDE solutions to experimental density data. Frequently, experimental data are only available over a limited

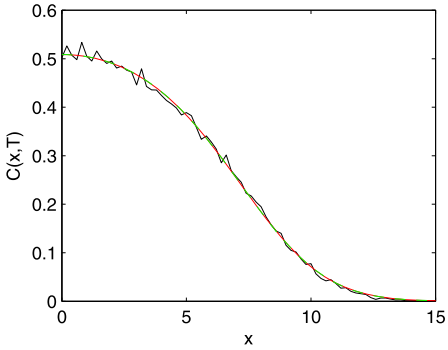

Fig. 6 The solutions of the lattice-free PDE model (*solid red*) and lattice-based PDE model (*dashed green*) with parameters adjusted to give the least-squares fit to averaged simulation data (*solid black*) from the discrete lattice-free model at time $T = 5$. The fitted solutions were obtained by minimising $R(\lambda, D, K)$ in Eq. (5). The initial condition is given by Eq. (4) with $C_0 = 0.2$, $x_0 = 5$. PDEs were solved on a domain of length $L = 30$ with mesh spacing $\delta x = 0.2$ (Color figure online)

Table 1 Parameters estimated by fitting the solutions of the lattice-based Fisher–Kolmogorov equation (Eq. (1) with Eq. (2)) and the lattice PDE (Eq. (1) with Eq. (3)) to averaged simulation data from the discrete lattice-free model at time $t = T$. Parameter values for the discrete simulation data: $\lambda = D = K = 1$. The initial condition is given by Eq. (4) with $C_0 = 0.2$, $x_0 = 5$. PDEs were solved on a domain of length $L = 30$ with mesh spacing $\delta x = 0.2$ ($N = 151$ mesh points). Parameters were estimated by minimising $R(\lambda, D, K)$ in Eq. (5). One unit of dimensionless time t corresponds to approximately 20 hours of real time. The RMSE column shows the root mean square error $\sqrt{(1/N)R(\lambda_{\text{fit}}, D_{\text{fit}}, K_{\text{fit}})}$ of the fitted solution

T	Lattice-based PDE				Lattice-free PDE			
	λ_{fit}	D_{fit}	K_{fit}	RMSE	λ_{fit}	D_{fit}	K_{fit}	RMSE
2.5	1.006	0.973	0.479	0.0024	1.055	0.931	0.960	0.0024
5.0	0.851	1.185	0.561	0.0047	0.961	1.031	1.050	0.0039
7.5	0.760	1.371	0.602	0.0113	0.946	1.047	1.057	0.0062
10.0	0.722	1.434	0.620	0.0200	0.989	0.967	1.036	0.0093

time scale or perhaps at only a few time intervals. Our results show that naively fitting the Fisher–Kolmogorov PDE at a single time point could result in what appears to be an excellent match to the data (e.g. Fig. 6), but give misleading parameter estimates (Table 1). Given the limitations on experimental timescales, it would be preferable to collect data at multiple time points and fit both the Fisher–Kolmogorov PDE and the lattice-free PDE developed here. The results in Table 1 indicate that the most suitable model could be the one for which parameter estimates remain relatively constant over different experimental durations.

5 Discussion and Conclusion

Previous investigations of a lattice-free model of cell motility, cell proliferation, and crowding effects were restricted to the special case where the cell density is spatially homogeneous. (Plank and Simpson 2012). This represents a relatively simple

tissue growth experiment where a population of cells is placed uniformly in a two-dimensional domain and the population remains spatially uniform throughout the experiment as the cell density increases to form a monolayer. This previous work established that the proliferation rate in the lattice-free framework is well approximated by Eq. (3) when the density is independent of spatial location. Many cell invasion assays, such as scratch assays and barrier assays, involve spatially variable initial conditions and cell density profiles. It is therefore important to extend the lattice-free framework to situations where the density is spatially variable, and test whether it can accurately describe such experiments.

In this work, we compared individual-based simulations of a lattice-free model of cell motility and cell proliferation with two PDE-based descriptions: the classical Fisher–Kolmogorov equation (Fisher 1937; Kolmogorov et al. 1937), which describes cell proliferation using a logistic source term; and an alternative PDE, which includes a linear diffusion term and a new source term that describes cell proliferation in the lattice-free framework (Plank and Simpson 2012). The solution of the PDE model with the new source term accurately matches averaged data from the lattice-free discrete model, while the solutions of the standard Fisher–Kolmogorov equation do not. Both PDE models give rise to travelling wave-like solutions with the same asymptotic wave speed; however, the lattice-free PDE predicts that the shape of the invasion wave is very different to that of the Fisher–Kolmogorov equation. The solutions of the lattice-free PDE model are not strictly travelling waves and we cannot perform the usual phase plane analysis to demonstrate the existence of a heteroclinic orbit joining the invaded and uninvaded steady states (Murray 2002). Instead, the new lattice-free PDE model acts like many other reaction–diffusion equations, such as Fisher's equation in an axi-symmetric geometry (Simpson et al. 2013a, 2013b), and does not formally support travelling wave solutions. Despite this, it is well accepted that the solutions of these kinds of models are very similar to travelling wave solutions (Murray 2002; Skellam 1951; Witelski et al. 2000).

Using the Fisher–Kolmogorov model to estimate parameters such as the proliferation rate, diffusivity and carrying capacity using a standard least-squares parameter estimation approach can give misleading results. The aim of this work is not to claim that the lattice-free PDE description is the correct description of invasion wave phenomena, nor that the standard Fisher–Kolmogorov model is an incorrect description of invasion wave phenomena. Instead, we aim to show that, when cells in the individual-based model are free to move and proliferate without being restricted to an artificial lattice, such as in the case of a cell invasion assay (Fig. 1), different outcomes are observed. Therefore, parameter estimates obtained by fitting standard, lattice-based models to experimental data should be treated with some caution. Interestingly, our analysis indicates that one key property of cell invasion, namely the speed of the invasion front, is unaffected by the removal of the lattice. This suggests that parameter estimation approaches focusing on invasion speed data should be more robust as they do not depend on the presence, or absence, of a lattice.

Acknowledgements This research was supported by the RSNZ Marsden Fund, grant number 11-UOC-005.

References

Anderson, A. R. A., & Chaplain, M. AJ. (1998). Continuous and discrete mathematical models of tumour-induced angiogenesis. *Bull. Math. Biol.*, *60*, 857–900.

Baker, R. E., & Simpson, M. J. (2010). Correcting mean-field approximations for birth-death-movement processes. *Phys. Rev. E*, *82*, 041905.

Bolker, B., & Pacala, S. W. (1997). Using moment equations to undersand stochastically-driven spatial pattern formation in ecological systems. *Theor. Popul. Biol.*, *52*, 179–197.

Bruna, M., & Chapman, S. J. (2012a). Excluded-volume effects in the diffusion of hard spheres. *Phys. Rev. E*, *85*, 011103.

Bruna, M., & Chapman, S. J. (2012b). Diffusion of multiple species with excluded-volume effects. *J. Chem. Phys.*, *137*, 204116.

Cai, A. Q., Landman, K. A., & Hughes, B. D. (2007). Multi-scale modeling of a wound-healing cell migration assay. *J. Theor. Biol.*, *245*, 576–594.

Callaghan, T., Khain, E., Sander, L. M., & Ziff, R. M. (2006). A stochastic model for wound healing. *J. Stat. Phys.*, *122*, 909–924.

Canosa, J. (1973). On a nonlinear diffusion equation describing population growth. *IBM J. Res. Dev.*, *17*, 307–313.

Caruso, A., Caselli, E., Fiorentini, S., Rotola, A., Prandini, A., Garrafa, E., Saba, E., Alessandri, G., Cassai, E., & Di Luca, D. (2009). U94 of human herpesvirus 6 inhibits in vitro angiogenesis and lymphangiogenesis. *Proc. Natl. Acad. Sci. USA*, *106*, 20446–20451.

Chapra, S. C., & Canale, R. P. (1998). *Numerical methods for engineers* (3rd ed.). Singapore: McGraw-Hill.

Chowdhury, D., Schadschneider, A., & Nishinari, K. (2005). Physics of transport and traffic phenomena in biology: from molecular motors and cells to organisms. *Phys. Life Rev.*, *2*, 318–352.

Codling, E. A., Plank, M. J., & Benhamou, S. (2008). Random walk models in biology. *J. R. Soc. Interface*, *5*, 813–834.

Deroulers, C., Aubert, M., Badoual, M., & Grammaticos, B. (2009). Modeling tumor cell migration: from microscopic to macroscopic models. *Phys. Rev. E*, *79*, 031917.

Druckenbrod, N. R., & Epstein, M. L. (2007). Behavior of enteric neural crest-derived cells varies with respect to the migratory wavefront. *Dev. Dyn.*, *236*, 84–92.

Dyson, L., Maini, P. K., & Baker, R. E. (2012). Macroscopic limits of individual-based models for motile cell populations with volume exclusion. *Phys. Rev. E*, *86*, 031903.

Fisher, R. A. (1937). The wave of advance of advantageous genes. *Ann. Eugen.*, *7*, 355–369.

Khain, E., Katakowski, M., Hopkins, S., Szalad, A., Zheng, X., Jiang, F., & Chopp, M. (2011). Collective behavior of brain tumor cells: the role of hypoxia. *Phys. Rev. E*, *83*, 031920.

Kolmogorov, A., Petrovsky, I., & Piscounov, N. (1937). Etude de léquation de la diffusion avec croissance de la quantité de matiere et son applicationa un probleme biologique. *Mosc. Univ. Math. Bull.*, *1*, 1–25.

Lagarias, J. C., Reeds, J. A., Wright, M. H., & Wright, P. E. (1998). Convergence properties of the Nelder–Mead simplex method in low dimensions. *SIAM J. Optim.*, *9*, 112–147.

Landman, K. A., & Fernando, A. E. (2011). Myopic random walkers and exclusion processes: single and multispecies. *Physica A*, *390*, 3742–3753.

Law, R., & Dieckmann, U. (2000). A dynamical system for neighbourhoods in plant communities. *Ecology*, *81*, 2137–2148.

Maini, P. K., McElwain, D. L. S., & Leavesley, D. I. (2004a). Traveling wave model to interpret a wound-healing cell migration assay for human peritoneal mesothelial cells. *Tissue Eng.*, *10*, 475–482.

Maini, P. K., McElwain, D. L. S., & Leavesley, D. (2004b). Travelling waves in a wound healing assay. *Appl. Math. Lett.*, *17*, 575–580.

Murray, J. D. (2002). *Mathematical biology I: an introduction* (3rd ed.). Heidelberg: Springer.

Nishiyama, C., Uesaka, T., Manabe, T., Yonekura, Y., Nagasawa, T., Newgreen, D. F., Young, H. M., & Enomoto, H. (2012). Trans-mesenteric neural crest cells are the principal source of the colonic enteric nervous system. *Nat. Neurosci.*, *15*, 1211–1218.

Othmer, H. G., Dunbar, S. R., & Alt, W. (1988). Models of dispersal in biological systems. *J. Math. Biol.*, *26*, 263–298.

Plank, M. J., & Simpson, M. J. (2012). Models of collective cell behaviour with crowding effects: comparing lattice-based and lattice-free approaches. *J. R. Soc. Interface*, *9*, 2983–2996.

Sengers, B. G., Please, C. P., & Oreffo, R. O. C. (2007). Experimental characterization and computational modelling of two-dimensional cell spreading for skeletal regeneration. *J. R. Soc. Interface*, *4*, 1107–1117.

Sengers, B. G., Please, C. P., Taylor, M., & Oreffo, R. OC. (2009). Experimental-computational evaluation of human bone marrow stromal cell spreading on trabecular bone structures. *Ann. Biomed. Eng.*, *37*, 1165–1176.

Shampine, L. F., & Reichelt, M. W. (1997). The MATLAB ODE suite. *SIAM J. Sci. Comput.*, *18*, 1–22.

Sherratt, J. A., & Murray, J. D. (1990). Models of epidermal wound healing. *Proc. R. Soc. Lond. B, Biol. Sci.*, *241*, 29–36.

Sherratt, J. A. (2000). Wavefront propagation in a competition equation with a new motility term modelling contact inhibition between cell populations. *Proc. R. Soc. Lond. Ser. A, Math. Phys. Sci.*, *456*, 2365–2386.

Simpson, M. J., Landman, K. A., & Hughes, B. D. (2010). Cell invasion with proliferation mechanisms motivated by time-lapse data. *Physica A*, *389*, 3779–3790.

Simpson, M. J., Baker, R. E., & McCue, S. W. (2011). Models of collective cell spreading with variable cell aspect ratio: a motivation for degenerate diffusion models. *Phys. Rev. E*, *83*, 021901.

Simpson, M. J., Treloar, K. K., Binder, B. J., Haridas, P., Manton, K., Leavesley, D. I., McElwain, D. L. S., & Baker, R. E. (2013a). Quantifying the roles of cell motility and cell proliferation in a circular barrier assay. *J. R. Soc. Interface*, *10*, 20130007.

Simpson, M. J., Binder, B. J., Haridas, P., Wood, B. K., Treloar, K. K., McElwain, D. L. S., & Baker, R. E. (2013b). Experimental and modelling investigation of monolayer development with clustering. *Bull. Math. Biol.*, *75*, 871–889.

Skellam, J. G. (1951). Dispersal in theoretical populations. *Biometrika*, *1/2*, 196–218.

Swanson, K. R., Bridge, C., Murray, J. D., & Alvord, E. C. Jr. (2003). Virtual and real brain tumors: using mathematical modeling to quantify glioma growth and invasion. *J. Neurol. Sci.*, *216*, 1–10.

Swanson, K. R., Harpold, H. L. P., Peacock, D. L., Rockne, R., Pennington, C., Kilbride, L., Grant, R., Wardlaw, J. M., & Alvord, E. C. Jr. (2008). Velocity of radial expansion of contrast-enhancing gliomas and the effectiveness of radiotherapy in individual patients: a proof of principle. *J. Clin. Oncol.*, *20*, 301–308.

Tremel, A., Cai, A., Tirtaatmadja, N., & Hughes, B. D. (2009). Cell migration and proliferation during monolayer formation and wound healing. *Chem. Eng. Sci.*, *64*, 247–253.

Witelski, T. P. (1994). An asymptotic solution for traveling waves of a nonlinear-diffusion Fisher's equation. *J. Math. Biol.*, *33*, 1–16.

Witelski, T. P. (1995). Merging traveling waves for the porous-Fisher's equation. *Appl. Math. Lett.*, *8*, 57–62.

Witelski, T. P., Ono, K., & Kaper, T. J. (2000). On axisymmetric traveling waves and radial solutions of semi-linear elliptic equations. *Nat. Resour. Model.*, *13*, 339–388.

Young, H. M., Bergner, A. J., Anderson, R. B., Enomoto, H., Milbrandt, J., Newgreen, D. F., & Whitington, P. M. (2004). Dynamics of neural crest-derived cell migration in the embryonic mouse gut. *Dev. Biol.*, *270*, 455–473.